Applied Physics B (2023) 129:150
https://doi.org/10.1007/s00340-023-08091-y

Applied Physics B
Lasers and Optics

RESEARCH

Thermal and spectroscopic characterization and evaluation of thermal effects for cryogenic cooled Yb:LuAG

Duo Zhu[1,3] · Yanjie Song[1,2,4] · Nan Zong[1,2,4] · Zhongzheng Chen[1,2,4] · Shenjin Zhang[1,2,4] · Fengfeng Zhang[1,2,4] · Yong Bo[1,2,4,5] · Qinjun Peng[1,2,4]

Received: 1 June 2023 / Accepted: 21 August 2023 / Published online: 6 September 2023

Abstract

Temperature dependent thermal and spectroscopic properties of Yb:LuAG crystal were presented in detail at temperature ranging from 298 to 77 K. We measured the thermal expansion coefficient, thermal conductivity and specific heat as functions of temperatures. Then, the thermal shock resistance parameters were evaluated, which were significantly increased from 0.75×10^6 to 10.19×10^6 W/m as temperature varies from 298 to 77 K. Moreover, the spectroscopic parameters, such as absorption and emission cross-sections and fluorescence lifetime were also determined. In order to evaluate Yb:LuAG's potential to generate high power laser output, a numerical model was employed by finite element method and ray tracing method. We simulated the temperature distribution in Yb:LuAG crystal slab when temperature reduces from 298 to 77 K. The maximum principal stress in slab decreases from 74.8 to 29.4 MPa and the maximum principal strain decreases from 23.76×10^{-5} to 7.63×10^{-5} for a given heat power of 1500 W with the temperature dropping from 298 to 77 K. The simulated near-field and far-field profiles of probe beam demonstrated a better beam quality at low temperature. These results indicate that cryogenically cooled Yb:LuAG is a promising laser medium for high power output while maintaining good beam quality

1 Introduction

Diode pumped solid-state lasers (DPSSL) with excellent beam quality and high output power are of great interest due to their important applications, including industrial, military and scientific research [1–4]. Ytterbium (Yb)-doped materials have received an increasing interest in recent years as efficient gain media for high power and high beam quality DPSSL since they have simple two-level energy manifolds, no up conversion, no excited state absorption and no concentration quenching [5]. In addition, Yb-doped materials have smaller quantum defect than widely used Nd-doped materials, which reduces thermal loading of the system. Yb:$Y_3Al_5O_{12}$ (Yb:YAG) is a kind of widely used Yb-doped laser material for the high power laser applications, however, it was found that as the Yb doping concentration in the YAG is increased, the thermal conductivity of the Yb:YAG drops significantly. Compared to Yb:YAG, Yb:$Lu_3Al_5O_{12}$ (Yb:LuAG) will have larger small signal gain and higher thermal conductivity as Yb doping concentration increase [6]. In recent years, some high Yb^{3+} doping concentration Yb:LuAG solid-state lasers have been demonstrated [7–11]. However, most studied have been performed at room temperature. For example, a Q-switched Yb:LuAG laser was reported at room temperature, delivering a maximum average power of 0.144 W and a pulse width of 193 ns [10]. In another work, an intra-cavity frequency-doubled Yb:LuAG thin-disk laser with Yb^{3+} doping concentration of 10% was

Duo Zhu and Yanjie Song have equally contributed to this work and should be regarded as co-first authors.

✉ Yanjie Song
songyanjie@mail.ipc.ac.cn

Yong Bo
boyong@mail.ipc.ac.cn

1 Key Lab of Solid State Laser, Technical Institute of Physics and Chemistry, Chinese Academy of Sciences, Beijing 100190, China

2 Key Lab of Functional Crystal and Laser Technology, Technical Institute of Physics and Chemistry, Chinese Academy of Sciences, Beijing 100190, China

3 University of Chinese Academy of Sciences, Beijing 100190, China

4 Institute of Optical Physics and Engineering Technology, Qilu Zhongke, Jinan 250000, China

5 Chinese Academy of Sciences, Beijing 100190, China

realized at room temperature, producing has an output powers of up to 1 kW at a wavelength of 515 nm with an optical conversion efficiency of 51.6%, unfortunately, it operated in multimode [11]. Further power scaling is limited due to thermal and optic characteristics in the Yb^{3+} doping laser gain medium at higher pump level. Yb-doped lasers are quasi-three-level lasers at room temperature for the thermally induced population of Yb^{3+}'s lower laser level, which causes significant problems such as the need to provide a significant pump density to reach transparency, a high pump threshold power, and the associated loss of efficiency [12, 13]. Fortunately, cooling down the Yb-doped gain media at cryogenic temperature could "freeze" the thermally induced population of the lower laser level and enable the "four-level" operation of lasers [14]. In addition, cryogenic cooling enables thermo-optic effects of the gain medium to be greatly reduced at a given power level, including higher thermal conductivity, lower thermal expansion, and thermo-optic coefficient [12], which are benefit to scale the output power and optical efficiency in solid-state laser systems [15]. For instantCE, for a diode pumped cryogenic 15 at.% Yb:LuAG laser, the output performed significantly better at 140 K with an output power 16 times and slope efficiency 7 times higher than the values at 240 K [16]. There results indicate that the cryogenic Yb:LuAG crystal has the potential to revolutionize high power and high beam quality lasers.

It is known to all that the simulation and design of laser systems highly dependent on the exact thermal and spectral data of the active medium. In past years, some thermal and spectral properties of Yb:LuAG crystal have been measured separately. For example, the thermal diffusivity, thermal conductivity, and beat capacity were given only at room temperature [17]. Following, the absorption and emission cross-sections of Yb:LuAG at cryogenic temperatures were investigated, but no any thermomechanical and thermal-optic properties were performed [18]. However, detailed thermal and spectroscopic data of Yb:LuAG crystal are not broadly available in wide temperature range from cryogenic temperature to room temperature, so far. In this letter, we systematically investigate the thermomechanical and spectroscopic properties in the temperature range across 77 to 298 K. Furthermore, a thermal model was employed to simulate the temperature distribution and stress distribution in a Yb:LuAG crystal slab for a given heat source as the temperature is cooled from 298 to 77 K. The maximum principal stress and principal strain are about three times smaller than room temperature. In addition, the simulated near-field (NF) and far-field (FF) profiles for a probe beam was analyzed by ray tracing method. The results indicate that the Yb:LuAG crystal slab operated at low temperature reached better beam quality. Consequently, Yb:LuAG crystal is a promising medium for generating high power laser with high beam quality simultaneously at low temperature.

2 Experimental investigation

The measurements presented below have been carried out using 10 at. % Yb^{3+}-doped Yb:LuAG crystals in the temperature range of 77 to 298 K. The crystals were grown with Czochralski method. The thermomechanical properties including thermal expansion coefficient, thermal conductivity, and specific heat. Thermal expansion and thermal conductivity were examined in a 6 mm × 6 mm × 20 mm Yb:LuAG crystal sample. Thermal expansion was measured using a thermal dilatometer (Linseis L75) with an uncertainty within ± 1%. Thermal conductivity was measured by a physical property measurement system (PPMS-9) with an uncertainty within ± 3%. The specific heat of Yb:LuAG crystal sample (3 mm × 3 mm × 1 mm) was also measured using another physical property measurement system (PPMS-14), and the accuracy of the present measurements is estimated to be within ± 1%.

The absorption, emission, and fluorescence spectra at different temperatures were measured by a fluorescence spectrometer (Edinburgh FLSP980) with resolution of 0.1 nm, here an OpoletteTM (OPO) 355 I laser was used as the pump source. For all the measurements, the sample was mounted in a cryostat, and the sample temperature was varied from 77 to 298 K. In order to measure the fluorescence lifetime, the sample was excited by laser pulse from the OpoletteTM (OPO) 355 I laser, and the fluorescence decay was observed by the fluorescence spectrometer, and the pinhole method has been adopted to eliminate the reabsorption [19]. The Yb:LuAG sample used in the spectrum measurements was cut into 10 mm diameter with 1 mm thickness and polished for both surfaces.

3 Results and discussion

3.1 Thermomechanical properties

Figure 1 shows the thermomechanical properties of Yb:LuAG crystal including thermal expansion coefficient, thermal conductivity, and specific heat at different temperatures. It wasIS found from Fig. 1a that the thermal expansion coefficients at room temperature is approximately 6.26×10^{-6}/K, which is slightly higher than undoped YAG and LuAG [19]. Then, the thermal expansion coefficient reduces with the drop of the temperature and down to 1.59×10^{-6} at 77 K, which is only about a quarter of that at room temperature. The thermal conductivity of the Yb:LuAG crystal is shown in Fig. 1b. The thermal

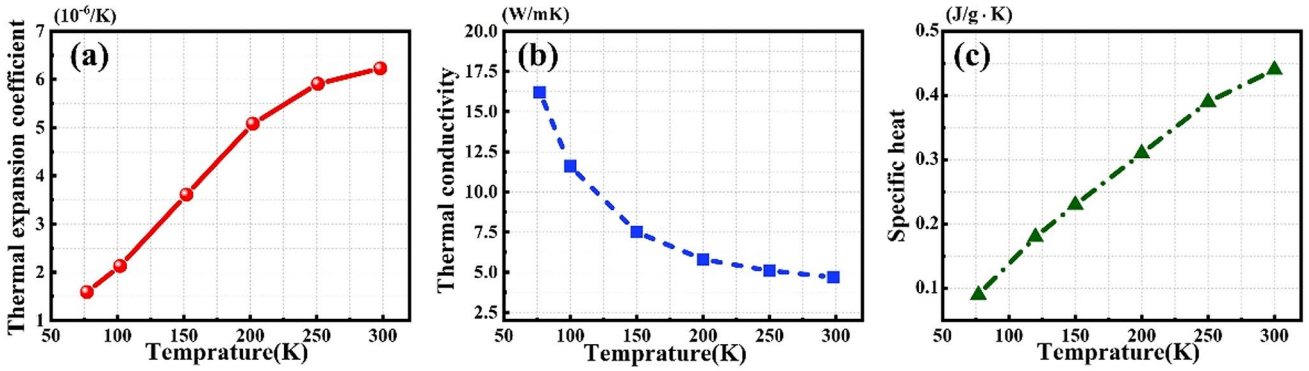

Fig. 1 Measured thermal expansion coefficient (**a**), thermal conductivity (**b**) and specific heat (**c**) of Yb:LuAG sample at different temperature from 77 to 298 K.3.2 Spectroscopic properties

conductivity significantly increases with the reduction in temperature, and its rising occurs more quickly at low temperature. For the sample at 298 K, the thermal conductivity is about 4.7 W/m K. When the temperature reduces to 77 K, the thermal conductivity increases to 16.2 W/m·K, which is 3.5 times higher than the value at room temperature. The measured thermal conductivity from 100 to 298 K are significantly smaller than thermal conductivity of undoped LuAG [20]. The measured specific heat versus temperature curves was shown in Fig. 1c, from which it can be seen that the specific heat decreases almost linearly with the temperature reduces. The specific heat value increased from 0.44 J/g·K to 0.09 J/g·K for the temperature from 298 to 77 K.

As well known, the parameter characterizing thermal shock resistance of crystal, R_T is proportional to the ratio of the thermal conductivity over the thermal expansion [17]. Therefore, high thermal conductivity and small thermal expansion coefficient are both required for high power laser materials. At room temperature, the R_T value of Yb:LuAG crystal is calculated to be only 0.75×10^6 W/m, and it is significantly larger at cryogenic temperatures than that at room temperature due to the small value of the thermal expansion coefficients and the high value of the thermal conductivity at low temperature. At 77 K, the R_T value is calculated to be 10.19×10^6 W/m with about 14 times bigger than that at room temperature, which is beneficial to the laser operation at high power level. Meanwhile, Yb:LuAG is also well suited for generating high power and high beam quality lasers at low temperature among several commonly used laser materials. Table. 1 summarizes the thermal shock resistance parameter R_T for some commonly used laser materials at cryogenic temperatures, and it can be seen that the thermal shock resistance of Yb:LuAG crystal is second only to 4 at.% Yb-doped YAG, and lager than other laser materials.

In order to make further evaluation on the laser performance of Yb:LuAG, the spectroscopic properties are measured and calculated. The absorption cross sections are usually calculated by Lambert Beer'sBeer-Lambert law [24], which can be described as:

$$\sigma_{abs} = \frac{2.303D(\lambda)}{N_0 l} \quad (1)$$

here, $D(\lambda)$ is the absorbance (optical density), N_0 is the density of dopant ions and l is the thickness of the sample. Figure 2a shows the absorption cross-sections of the Yb:LuAG

Table 1 Comparison of thermal properties of several laser materials at cryogenic temperature [20–23]

Laser material	Thermal conductivity (W/m·K)	Coefficient of thermal expansion (10^{-6}/K)	Thermal shock resistance (10^{-6} W/m)
10 at.% Yb:LuAG 77 K	16.2	1.59	10.19
4 at.% Yb:YAG 100 K	25	1.95	12.82
15 at.% Yb:YAG 100 K	16.4	1.95	8.41
5 at.% Yb:YLF 100 K *a* axis	11.3	2.36	4.79
BYF 100 K *b* axis	9.7	9.5	1.02
3 at.% Yb:CaF_2 123 K	6	8.1	0.74
9 at.% Yb:Sc_2O_3 88 K	7	1.055	6.64
GSAG 83 K	11.6	1.88	6.17

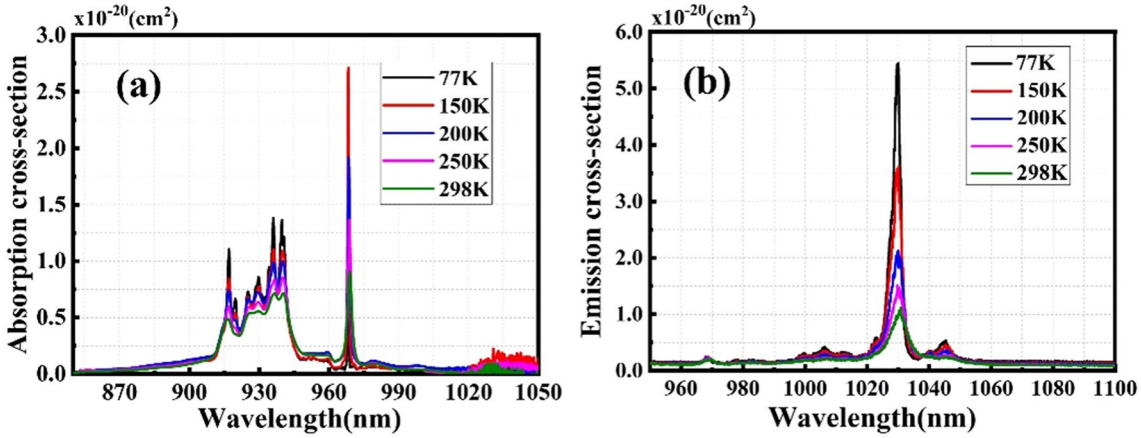

Fig. 2 Measured absorption cross sections (**a**), emission cross sections (**b**) for selected temperatures

crystal at given temperatures respectively, and the data have been corrected for Fresnel losses on the surface. As shown in Fig. 2a, the absorption band ranging from about 915–940 nm decomposes into several peaks at low temperatures, which is similar to Yb:YAG [14]. It can be seen that almost all absorption peaks in the pump band show a reduction in bandwidth and become more intense as temperature is lowered with the exception of the data at 77 K near 968 nm, which is anomalous. While line narrowing continues to happen as temperature is lowered, the sharp absorption cross-sections peak linewidth cannot be resolved and appears as a line of reduced intensity. Considering the absorption band near 940 nm, there are two peaks at 939.7 nm and 940.6 nm, respectively. The peak absorption cross-sections at 939.7 nm and 940.6 nm are 1.37 and 1.22×10^{-20} cm2 at 77 K, which are about 1.9 and 1.71 times higher than that at room temperature.

The Füchtbauer-Ladenburg equation is the common formula used to calculated spectral dependent stimulated emission-cross sections [25], supposing reabsorption can be neglected, it can be described as:

$$\sigma_{em}(\lambda) = \frac{\lambda^5 I(\lambda)}{8\pi n^2 c\tau \int \lambda I(\lambda) d\lambda} \tag{2}$$

here $I(\lambda)$ is the spectral intensity of emission of the Yb^{3+}ions, τ is the measured lifetime of the upper laser level, c is the velocity of light in vacuum, and n is the refractive index at the emission wavelength. As shown in Fig. 2b, the emission cross-sections exhibit a trend for evolving strong peaks with significantly higher peak cross sections at lower temperatures. The emission cross-section at 1030 nm is 5.13×10^{-20} cm^2 at 77 K, which is 5.43 times higher than that at room temperature. In addition, the full width at half maximum (FWHM) bandwidth is reduced from about 8.39 nm to about 3.63 nm as the temperature decreases from 298 to 77 K. The peak emission wavelength is 1030.9 nm at 298 K and shifts only slightly to 1030.1 nm at 77 K. The fluorescence lifetime at 77 K, 150 K, 200 K, 250 K and 298 K is also characterized by a single exponential decay function and the results are shown in Fig. 3. It could be seen that the fluorescence lifetime significantly is decreased for lower temperatures, resulting from the changing of Boltzmann populations at lower temperatures. The fluorescence lifetime at 298 K is about 1.74 times larger than that at 77 K.

4 Numerical simulation

Based on the measured thermal properties mentioned above, a numerical modeling of thermal-steady-state for a slab crystal was established at different temperatures in order to evaluate the potential to high power high beam quality lasers.

Figure 4 shows the three-dimensional (3D) Yb:LuAG crystal slab modeling, the slab size is $180\times70\times7$ mm.

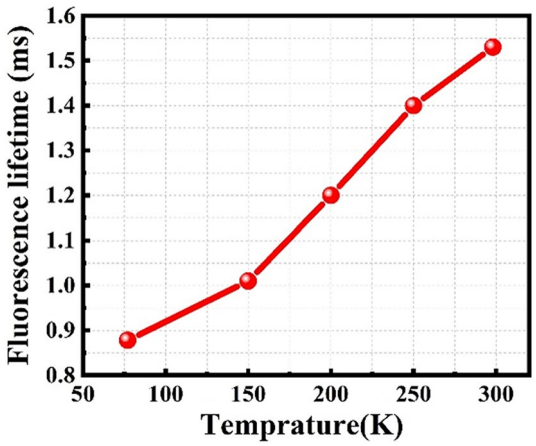

Fig. 3 Measured fluorescence lifetime for selected temperatures

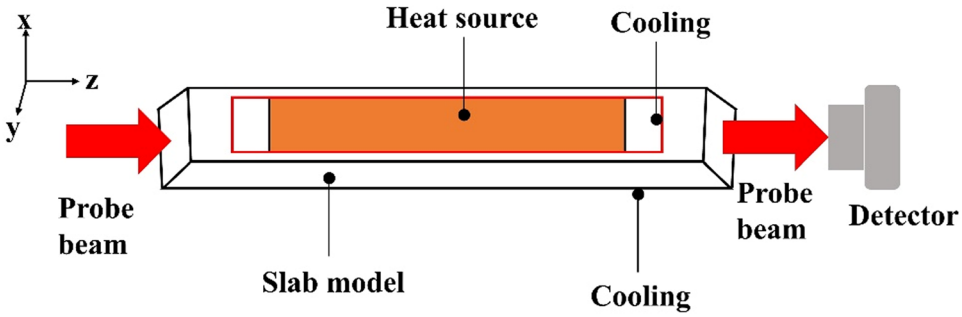

Fig. 4 Schematic diagram of Yb:LuAG slab crystal numerical model for heat and probe

Furthermore, the probe beam is a rectangular parallel shape of 10 × 60 mm, which is incident to the front edge facet and travels in the slabs along the zigzag path. The general steady-state heat equation for an anisotropic slab crystal in Cartesian coordinates is given by following:

$$k_x\frac{\partial^2 T(x,y,z)}{\partial x^2}+k_y\frac{\partial^2 T(x,y,z)}{\partial y^2}+k_z\frac{\partial^2 T(x,y,z)}{\partial z^2}+Q_v(x,y,z)=0 \tag{3}$$

which $T(x,y,z)$ is temperature, k_x, k_y and k_z are three different thermal conductivities along x, y, and z axes, respectively, and $Q_v(x,y,z)$ is the heat source density in watts per unit volume. Here $Q_v(x,y,z)$ can be written Q_0, which is the central source term in the crystal and equal to 0.3125 W/mm^3. The medial area (orange color in Fig. 4) of the slab that absorbs the pump light is considered as a heat source, and the total heating power is 1500 W.

There exist the complex heat convection boundary conditions of all faces in the laser system, but here a simplified case is adopted. In this case, the medial part (red box) of two large surfaces were cooled via coolant at different temperatures, and other surfaces were cooled by air convection. The heat convection boundary condition can be described as:

$$k_x\frac{\partial T(x,y,z)}{\partial x}|_{x=x_0}=h\left(T\left(x_0,y,z\right)-T_0\right) \tag{4}$$

$$k_y\frac{\partial T(x,y,z)}{\partial y}|_{y=y_0}=h\left(T\left(x,y_0,z\right)-T_0\right) \tag{5}$$

$$k_z\frac{\partial T(x,y,z)}{\partial z}|_{z=z_0}=h\left(T\left(x,y,z_0\right)-T_0\right) \tag{6}$$

which $T(x,y,z)$ is the temperature distribution in the slab surfaces, h and T_0 are the heat transfer coefficient and temperature of coolant, respectively. The heat transfer coefficient of coolant is 15,000 W/m^2·K.

The temperature distribution is calculated by Ansys. The maximum temperature point is located in the center of the slab while the minimum temperature point is located near the top corner of the bottom surface in the slab. Figure 5 shows that the simulated maximum temperature difference

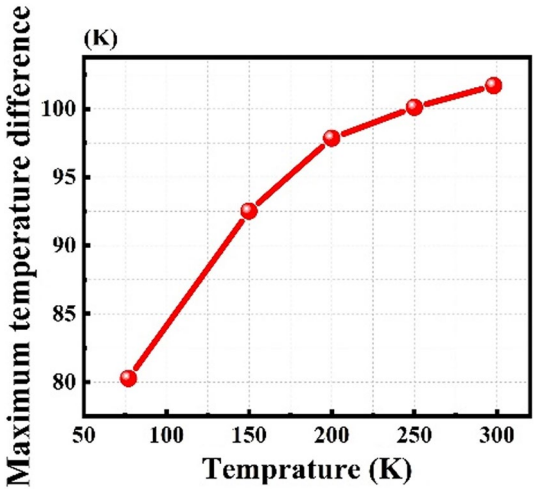

Fig. 5 Simulated temperature difference in Yb:LuAG crystal slab versus different cooling temperature from 77 to 298 K

in Yb:LuAG slab versus cooling temperature. It can be seen from Fig. 5 that the temperature difference decreases from a maximum value of 101–80 ℃ when the cooling temperature changes from 298 to 77 K, which means that the temperature gradient is lower at low temperature.

The inhomogeneous heat source and cooling cause a non-uniform temperature distribution, resulting in the thermal stress in the crystal slab. The finite element (FEM) method(FEM) is also adopted to calculate the thermal stress distribution. Figure 6 shows the 3D principal stress and principal strain distribution in Yb:LuAG slab at room temperature. It's easy to see that the maximum points of principal stress and principal strain are distributed in the four corners of the pump area in top surface, which is similar at other cooling temperatures. Figure 7 shows the simulated maximum principal stress (red) and maximum principal strain (blue) in Yb:LuAG crystal slab versus different cooling temperatures. It suggests that the maximum principal stress in Yb:LuAG crystal slab decreases rapidly as the cooling temperature drops. The maximum principal stress in crystal slab is 29.4 MPa while the cooling temperature is 77 K, which is about lower two times than that at room temperature. The maximum output power of the laser is limited by the stress

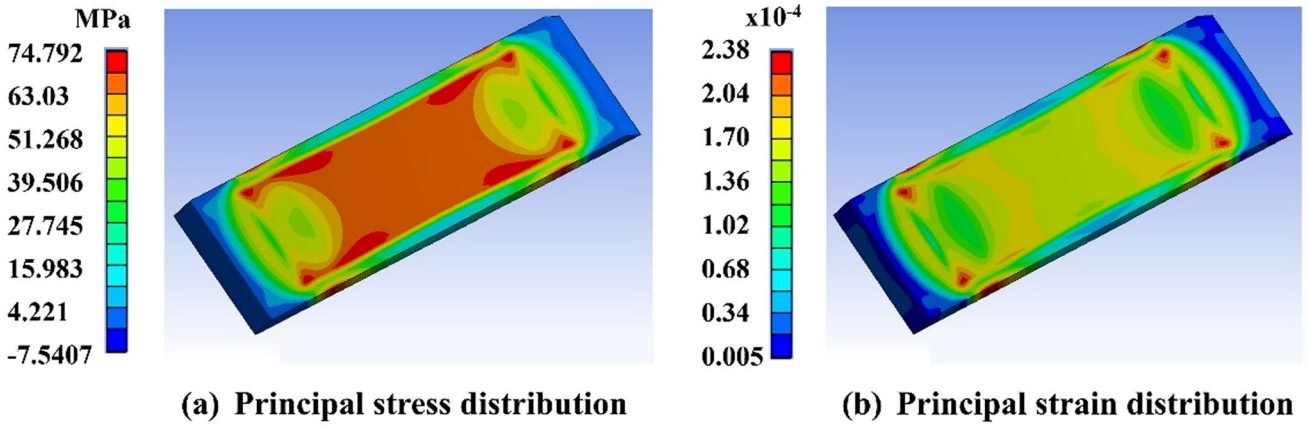

Fig. 6 Simulated typical 3D principal stress (**a**) and 3D principal strain (**b**) distributions in Yb:LuAG crystal slab at room temperature

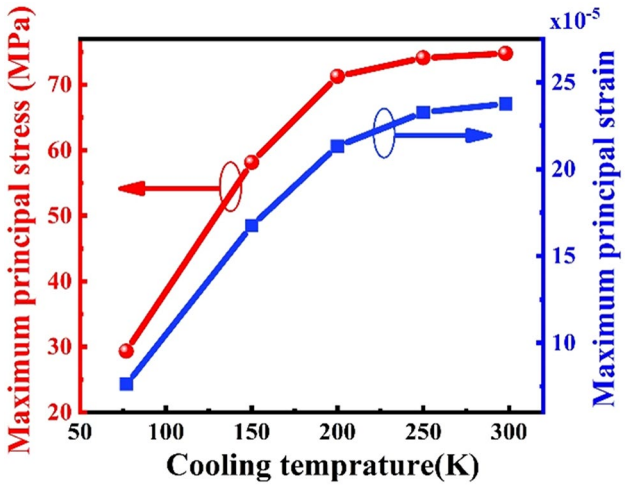

Fig. 7 Simulated maximum principal stress (red) and maximum principal strain (blue) in Yb:LuAG crystal slab versus different cooling temperature

fracture [26], therefore, smaller thermal stress is beneficial to laser power scaling. Furthermore, the surface deformation due to strain contributes greatly to the deterioration of the beam quality of the output laser [27]. It can be seen in Fig. 7 that the trend of the maximum principal strain is similar to the maximum principal stress, over the temperature range from 77 to 298 K. The maximum principal strain is 7.63×10^{-5} at the cooling temperature of 77 K, which is about lower three times than that at room temperature.

Aberration due to thermal deformation of laser beam is an important factor affecting the beam quality. In order to analyze the influence of different cooling temperature on beam quality, the near-field and far-field profiles for a probe beam through the Yb:LuAG crystal slab at different cooling temperatures are simulated by ray tracing. The probe beam at 1030 nm is incident to the front edge facet of the slab model and travels in the slabs along the zigzag path. Figure 8 shows the simulated two dimensional (2D) near-field and far-field profiles of probe beam through the crystal slab at different cooling temperatures. It is found that the aberrations due to thermal deformation deteriorates sharply as the cooling temperature changes from 77 to 298 K. It can be seen that there is no obvious indication of optical distortions in near-field profile when the cooling temperature is 77 K, meanwhile, a distinct bright line could be seen in the center of near-field profile when the cooling temperature is 250 K and 298 K. In addition, it can be seen that the far-field spot gradually converges into a small spot with the cooling temperature decreases, which demonstrates that Yb:LuAG slab lasers operated at low temperature reached better beam quality [28, 29]. Therefore, cryogenic cooled Yb:LuAG lasers are suitable for high power high beam quality lasers.

5 Conclusion

In conclusion, we have presented a detailed data of thermal expansion, thermal conductivity and specific heat for Yb:LuAG crystal from 77 to 298 K. Then, the enhanced thermal shock resistance parameter calculated, indicating that the Yb:LuAG laser operated at cryogenic temperatures exhibit a higher resistance to stress fracture. Meanwhile, the absorption spectra, emission spectra, and fluorescent lifetime were measured in the temperature range 77 K to 298 K. The absorption and emission cross-sections both exhibit a trend for evolving strong peaks with significantly higher peak cross sections at lower temperatures. Based on the measured thermal data mentioned above, a thermal model was employed to simulate the temperature, stress and strain distributions in a Yb:LuAG slab for different temperatures from 298 to 77 K. The maximum principal stress and principal strain are about three times smaller

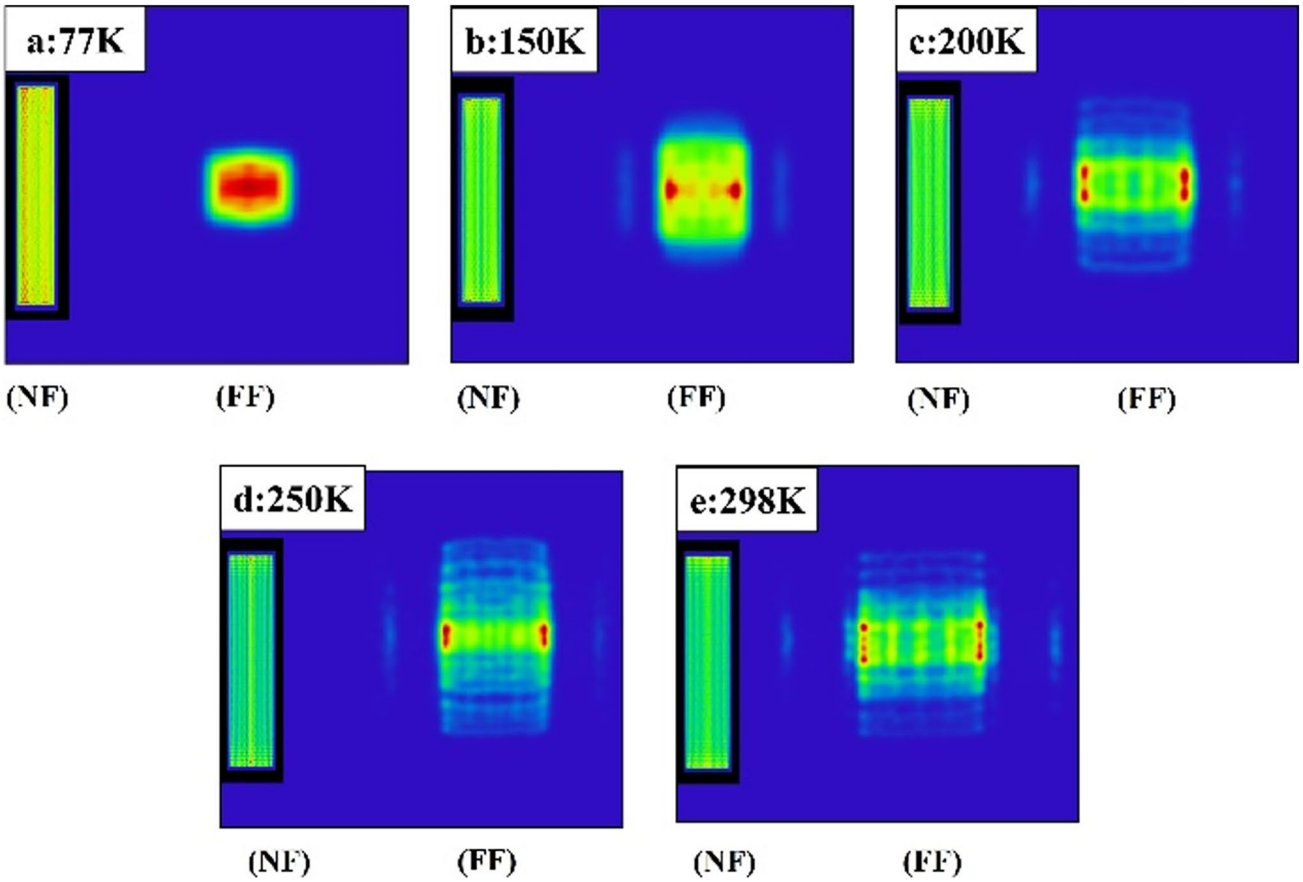

Fig. 8 Simulated 2D NF and FF intensity distribution for a rectangular probe beam at 1030 nm at different cooling temperatures; **a** 77 K; **b** 150 K; **c** 200 K; **d** 250 K; **e** 298 K

than room temperature, which shows that cryogenic cooled Yb:LuAG lasers are suitable for high power with high beam quality simultaneously.

Acknowledgements This work was funded by National Natural Science Foundation of China (NSFC) (62205349), the West Light Foundation of CAS (xbzg-zdsys-202018) and National special support program for high-level talent science and technology (No. SQ2022RA24910010).

Author contributions Author contributions: Duo Zhu and Yanjie Song wrote the main manuscript text. Nan Zong and Zhongzheng Chen contributed to the writing-review & editing. Shenjin Zhang, Fengfeng Zhang, Yong Bo and Qinjun Peng supervised and led the planning and implementation of research activities. All authors reviewed the manuscript.

Data availability The data that support the findings of this study are available on request from the corresponding author, [Yanjie Song], upon reasonable request.

Declarations

Conflict of interest The authors declare no conflicts of interest.

References

1. X. Cao, W. Wallace, C. Poon, J.-P. Immarigeon, Mater. Manuf. Process. **18**, 1–22 (2003)
2. P. Sprangle, B. Hafizi, A. Ting, R. Fischer, Appl. Opt. **54**, F201–F209 (2015)
3. H. Rui, S. Zhao, X. Jie, J. Wu, S. Fang, Opt. Appl. **39**, 251–265 (2009)
4. A. Extance, Military technology: laser weapons get real. Nature **521**, 408–410 (2015)
5. D. Luo, J. Zhang, C. Xu, H. Yang, H. Lin, H. Zhu, D. Tang, Opt. Mater. Express **2**, 1425–1431 (2012)
6. B. Jiang, X. Lu, Y. Zeng, S. Liu, J. Li, W. Liu, Y. Shi, Y. Pan, Phys. Status Solidi C **10**, 958–961 (2013)
7. A. Brenier, Y. Guyot, H. Canibano, G. Boulon, A.G. Petrosyan, J. Opt. Soc. Am. B **23**, 676–683 (2006)
8. A. Pirri, G. Toci, M. Nikl, V. Babin, M. Vannini, Opt. Express **22**, 4038–4049 (2014)
9. J. Dong, K.-I. Ueda, A.A. Kaminskii, Opt. Lett. **32**, 3266–3268 (2007)
10. S. Lv, C. Gao, Z. Tian, X. Su, B. Zhang, Opt. Commun. **478**, 126356 (2020)

11. T. Dietrich, S. Piehler, M. Rumpel, P. Villeval, D. Lupinski, M. Abdou-Ahmed, T. Graf, Opt. Express **25**, 4917–4925 (2017)
12. T.Y. Fan, D.J. Ripin, R.L. Aggarwal, J.R. Ochoa, B. Chann, M. Tilleman, J. Spitzberg, IEEE J. Quantum Electron **13**, 448–459 (2007)
13. D.C. Brown, IEEE J. Quantum Electron **11**(3), 587–599 (2005)
14. J. Körner, V. Jambunathan, J. Hein, R. Seifert, M. Loeser, M. Siebold, U. Schramm, P. Sikocinski, A. Lucianetti, T. Mocek, Appl. Phys. B **116**, 75–81 (2014)
15. D.J. Ripin, J.R. Ochoa, R. Aggarwal, T.Y. Fan, Opt. Lett. **29**, 2154–2156 (2004)
16. S.P. David, V. Jambunathan, F. Yue, A. Lucianetti, T. Mocek, Opt. Laser Technol. **135**, 106720 (2021)
17. J. Petit, B. Viana, P. Goldner, J.-P. Roger, D. Fournier, J. Appl. Phys **108**, 123108 (2010)
18. D.C. Brown, C.D. Mcmillen, C. Moore, J.W. Kolis, V. Envid, J. Lumin. **148**, 26–32 (2014)
19. H. Kühn, S.T. Fredrich-Thornton, C. Kränkel, R. Peters, K. Petermann, Opt. Lett. **32**, 1908–1910 (2007)
20. R.L. Aggarwal, D.J. Ripin, J.R. Ochoa, T.Y. Fan, J. Appl. Phys. **98**, 103514 (2005)
21. B.L. Garrec, V. Cardinali, G. Bourdet, Proc. SPIE. **8780**, 87800E (2013)
22. V. Cardinali, E. Marmois, B.L. Garrec, G. Bourdet, Opt. Mater. **34**, 990–994 (2012)
23. D. Rand, D. Miller, D.J. Ripin, T.Y. Fan, Opt. Mater. Express. **1**, 434–450 (2011)
24. L. Tian, S. Wang, K. Wu, B. Wang, H. Yu, H. Zhang, H. Cai, H. Huang, Opt. Mater. **36**, 521–528 (2013)
25. S. Ding, F. Peng, Q. Zhang, J. Luo, W. Liu, D. Sun, R. Dou, J. Gao, G. Sun, M. Cheng, J. Alloys Compd. **693**, 339–343 (2017)
26. D.C. Brown, S. Tornegård, J. Kolis: High Power Laser Sci. Eng. **4**, e15 (2016)
27. P. Ferrara, M. Ciofini, L. Esposito, J. Hostaa, L. Labate, A. Lapucci, A. Pirri, G. Toci, M. Vannini, L.A. Gizzi, Opt. Express **22**, 5375–5386 (2014)
28. Y. Ping, L. Xiang, N. Yu, L. Dong, X. Bing, Proc. SPIE **7843**, 784327 (2010)
29. C. Shao, Y. Guo, Z. Chen, Y. Bo, Y. Li, L. Zhang, L. Yuan, Y. Xu, S. Meng, Q. Peng, Opt. Express **28**, 8056–8063 (2020)